JMEPEG (2011) 20:544–550
DOI: 10.1007/s11665-011-9878-3

1059-9495/$19.00

Functional Characterization of Shape Memory CuZnAl Open-Cell Foams by Molten Metal Infiltration

S. Arnaboldi, P. Bassani, F. Passaretti, A. Redaelli, and A. Tuissi

(Submitted June 16, 2010; in revised form January 31, 2011)

In the recent years, the research for novel materials with tailored mechanical properties, as well as functional properties, has encouraged the study of porous and cellular materials. Our previous work proposed and reported about the possibility to manufacture open-cell metal foams of CuZnAl shape memory alloy by liquid infiltration in a leachable bed of silica-gel particles. This innovative methodology is based on cheap commercial consumables and a simple technology, focusing on intermediate-density low-cost foams with interesting cost/benefits ratio. Microstructural analyses on foamed specimens showed uniform microstructure of ligaments and a very regular and well reproducible open-cell morphology. Moreover, calorimetric analysis detected a thermo-elastic martensitic transformation in the foamed material. In this study, a CuZnAl shape memory alloy was considered and tested to clarify possible effects of the foaming process on the functional properties of the material. Morphological, calorimetric, and thermo-mechanical analyses were carried out. The results show that it is possible to produce metal foams of CuZnAl shape memory alloy with different functional properties and able to recover mono-axial compressive strains up to 3%.

Keywords CuZnAl shape memory alloys, metal foam, stress-temperature-induced martensitic transformation

1. Introduction

Metal foams are an innovative and challenging class of materials. Due to their unusual physical, mechanical, thermal, and acoustic properties (Ref 1-4), they have been granted much attention by materials researchers in the last few years and are finding several structural and functional applications in different engineering fields (Ref 5, 6).

The most widely available commercial foams are aluminum-based, since they offer lightness, high stiffness, good thermal stability, and quite low manufacturing cost (Ref 6-9). However, several other metals and alloys can now be foamed quite easily (i.e., Fe-base alloys, titanium, nickel) and the continuous effort to improve manufacturing technologies will soon allow tailored cellular and porous materials to be synthesized, to satisfy the ever increasing specificity of designers' needs (Ref 10).

The relative quantities and distribution of metal and voids in the foam can be adjusted to obtain the desired stiffness, permeability, and thermo-physical properties (Ref 5). The main parameters to be considered are the relative density of the foamed material, as well as the size, distribution, and interconnection of the pores. Nowadays the processes used for manufacturing porous materials, generally limit the achievable ranges of those parameters; on the other hand, great effort is devoted to enhance the resulting microstructural homogeneity, to make the production more reliable and reproducible and to reduce the morphological stochasticity (Ref 5, 11).

In a previous work by our group, an innovative methodology for the manufacturing of copper-based open-cell metal foam (sponge) was proposed and developed (Ref 12). It introduced the use of amorphous SiO_2 beads (Silica-gel) as space holders, for production through molten metal infiltration. Once infiltrated, SiO_2 particles are dissolved by a wet solution of hydrofluoric acid (HF). By this route, highly homogeneous foams, having almost spherical open-cell morphologies, can be produced. The proposed methodology was based on cheap commercial consumables and a simple technology, focusing on intermediate-density low-cost foams with interesting cost/benefit ratios. The use of SiO_2 beads as space holder yields cellular metals with a very homogeneous arrangement of almost spherical cavities and, because of the high chemical stability of SiO_2, no reactions between space holders and molten metal were observed. Besides, the same process was adopted to manufacture a CuZnAl shape memory alloy (SMA) sponge (Ref 13). Apart from the NiTi-based SMAs, the Cu-based SMAs are the only subclass of these alloys to have found practical commercial applications. However, as it is well known, Cu-based SMAs tend to show excessive grain growth when heat-treated, and, generally, are prone to aging effects. In fact, the betatization heat treatment, necessary to improve and stabilize the functional properties of the material, induces a metastable β structure (either β2 or β3) in a temperature range where α and γ phases are thermodynamically stable. The aging process, which consists in the precipitation of equilibrium phases, could cause several problems, such as martensite stabilization, degradation of shape memory effect, or intergranular cracking (Ref 14-19).

It has been observed that the foaming process enhance and stabilize the thermo-mechanical properties of the material, as

This article is an invited paper selected from presentations at Shape Memory and Superelastic Technologies 2010, held May 16-20, 2010, in Pacific Grove, California, and has been expanded from the original presentation.

S. Arnaboldi, P. Bassani, F. Passaretti, A. Redaelli, and **A. Tuissi**, Institute for Energetics and Interphases, Corso Promessi Sposi 29, Lecco, Italy. Contact e-mail: sergio.arnaboldi@ieni.cnr.it.

the geometrical constraints due to the foam morphology are able to limit the grain growth (Ref 13).

In this work, the same CuZnAl shape memory alloy was considered and tested to clarify possible effects of the foaming process on the functional properties of the material. Several sponge samples were manufactured using silica-gel beads of different sizes. The morphological, calorimetric, and thermo-mechanical properties of the various processed foams were investigated and correlated.

The achieved results seem to confirm the feasibility and interest of producing novel metal foams, which could widen the current asset of possible applications. Thus, the possibility to obtain a relatively broad range of smart foams with tailored functional properties, able to combine the peculiarity of SMAs and the functionality of metal foams, was experimentally evaluated and demonstrated.

2. Experimental

The material tested in this work was a typical CuZnAl SMA. The chemical composition and some physical properties of the considered alloy are reported in Table 1. Several ingots (60 mm in diameter, and 25 mm in height) of the desired composition were melted in an *Aseg-Galloni VCMIII* induction melt casting machine, under pure Ar flow at room pressure.

The small cylinders of SMA, adding up to almost 30% of the final foam volume, were processed and foamed through the methodology previously proposed (Ref 13).One of the ingots was considered as reference bulk material (BM), while the others were foamed using amorphous SiO_2 beads (commercial non-indicating Sigma S7500 Type II), statistically different in mean diameter size: 2.5, 3.5, 4.5 mm. Thus, three CuZnAl foams (F1, F2, and F3), with different pores size, were manufactured (Fig. 1).

After complete solidification and cooling, the resulting solids (silica-gel beads plus infiltrated SMA) were unmolded and lathe machined to their final shape. The foam samples were immersed in an aqueous HF bath (25 vol.%) till complete SiO_2 dissolution was achieved. The material was heat-treated in a kiln (830 °C; 15′) under Ar atmosphere and quenched in water at room temperature (betatization treatment). Both, bulk and foam ingots, were cut using a conventional system (abrasive disk and milling cutter) and several samples were prepared for metallographic observation. The surfaces of the specimens were polished and analyzed under an optical microscope, to evaluate microstructural and morphological features: some of them were etched with an H_2O_2-NH_4OH aqueous solution and observed under non-polarized light; others were analyzed under polarized light without etching of the surface. The sample composition was investigated using a scanning electron microscope, equipped with energy dispersive spectroscopy (EDS) microanalysis system, to estimate the actual chemical composition of the processed material, and evaluate possible shifts in zinc quantity, which can occur due to an excessive evaporation of this element during the melting process.

Table 1 Chemical composition and physical properties of the investigated SMA

Chemical composition, wt.%			Physical properties	
Cu	Zn	Al	Melting temperature, °C	Density, g/cm^3
72.5	21.5	6	920	8.16

Foam porosity was estimated in two ways: first, by the analysis of digital images of flat sections, exploiting the fact that bi-dimensional porosity is equal to the tridimensional one (p) for a random distribution of pores (Ref 20); second, by weighing and measuring prismatic specimens. Porosity and relative density of the different foams were easily evaluated as follows:

Relative foam density:

$$\rho_{rel} = \frac{\rho_{foam}}{\rho_{bulk}} \quad \text{(Eq 1)}$$

Porosity (%):

$$p = 1 - \rho_{rel} \quad \text{(Eq 2)}$$

where ρ_{foam} and ρ_{bulk} represent foamed and bulk material density, respectively. Calorimetric analyses were carried out in a *TA Instruments Q100* differential scanning calorimeter at a cooling/heating rate of 10 °C/min in a temperature range between −100 and 80 °C, which includes the direct and reverse transformations.

Moreover, several compression specimens were prepared. BM and F1, F2, F3 foams were sectioned following the scheme reported in Fig. 2. The dimensions of the specimens (height-to-thickness ratio: 1:5), were kept as small as applicable,

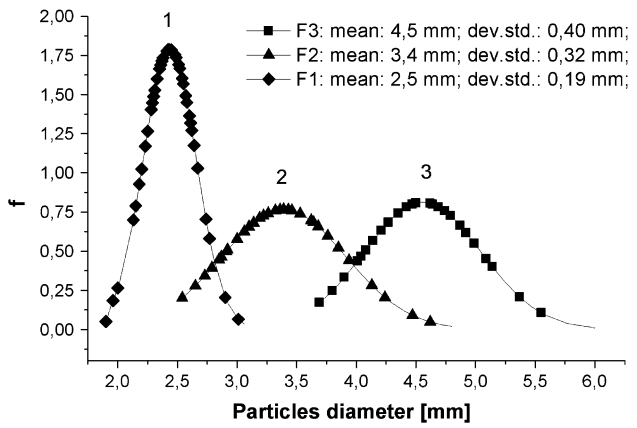

Fig. 1 Granulometry (normal distribution f) of SiO_2 beads used as space holders

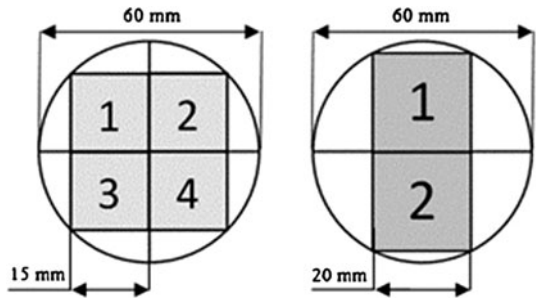

Fig. 2 Compression specimens cutting setup: (a) BM and F1 specimens; (b) F2 and F3 specimens

considering the necessity to minimize size effects and obtain reliable and reproducible results. The tests were carried out on an *MTS Alliance RF/150* universal testing machine, equipped with a 150 kN load cell, extensometers with 25 or 50 mm gauge length and a thermostatic chamber, necessary to set and control the test temperature. The system was configured to perform pseudo-elasticity (PE) and shape memory effect (SME) tests, to characterize thermo-mechanical properties of the foams under different conditions.

PE tests were carried out at constant temperature above A_f, cyclically loading and unloading the material in compression, while increasing the value of final applied strain at every cycle. SME tests consisted in different steps: (a) material cooling from $T_0 > A_f$ down to $T_1 < M_f$; (b) isothermal loading at temperature T_1, to a preset level of strain (usually 3% or 5%); (c) heating to T_0. A small preload was kept constant during the cooling and heating steps.

To estimate the strain-recovery, load and strain were monitored through the output signals of the machine during the entire test, while temperature was recorded by an independent thermocouple (K type), applied, where possible, on the surface of the sample.

3. Results and discussion

3.1 Morphology and microstructure

A series of CuZnAl foams, different in cell size, were processed and characterized. Typical sections of the prepared foams are shown in Fig. 3 and 4.

As can be seen, silica-gel beads were completely dissolved by HF, without optical evidence of any significant metal corrosion. From these images, it is possible to appreciate that the silica-gel beads did not undergo any change in their initial shape/size during either metal infiltration or solidification. Moreover, as the internal surface of the cells is a "negative image" of the surface morphology of the silica-gel spheres, it is possible to state, that the size distribution of cells and space holders, can be considered to be formally the same (Fig. 5).

The three processed foams showed small interconnection windows between adjacent pores. This means that, during the infiltration process, the silica gel beads used as space holders, were not completely wetted by molten brass, which left part of the interstitial space unfilled. This phenomenon induces open-cell morphology in the foamed state, necessary to obtain complete dissolution of the space holders.

SEM and EDS microanalyses show an excellent homogeneity of the chemical composition both in bulk and in foamed specimens. Moreover, analyses show no reaction products or inter-diffusive phases between metal and space holder spheres, and no traces of Si or O were detected in the metal meshwork after SiO_2 leaching.

The microstructure of the as-cast samples was often characterized by the presence of precipitates of the equilibrium phase α. This phase grows from β grain boundaries in a rod-like shape, because, after solidification, the alloy remains in the α + β field during cooling. This phase has an fcc structure and has a lower content of alloying elements (Ref 14). When etched and observed under a conventional optical microscope, it appears brighter than the β phase. After the betatization treatment, the microstructure becomes homogeneous and, as the alloy is in the austenitic phase at room temperature, it consists of isotropic grains of phase β (Fig. 6).

As it is well known, phase β has a B2 (called β_2, CsCl type) or $L2_1$ (called β_3, Cu_2AlMn type) structure, which is formed from B2 through an orientation reaction below a transition

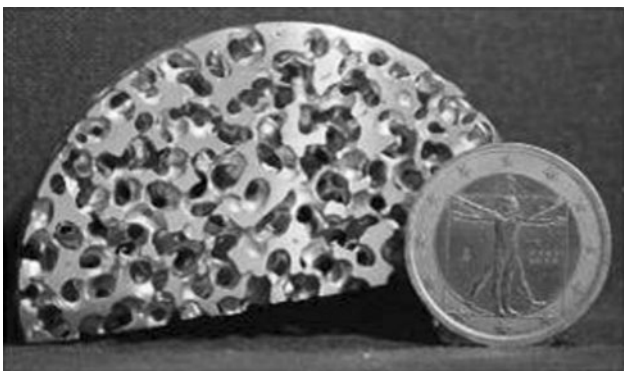

Fig. 3 Image of a CuZnAl open cell foam sample

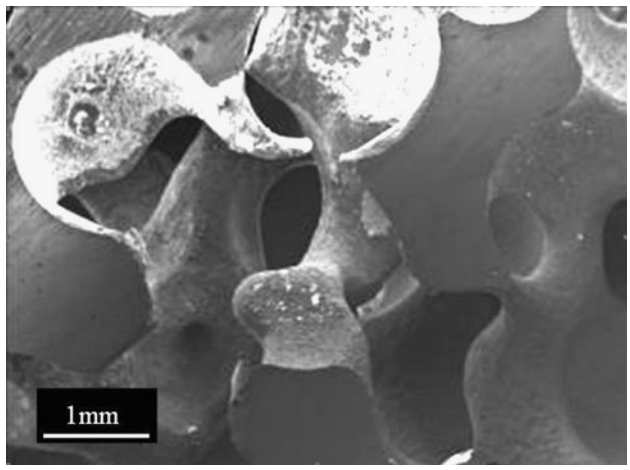

Fig. 4 SEM image of CuZnAl polished specimen surface

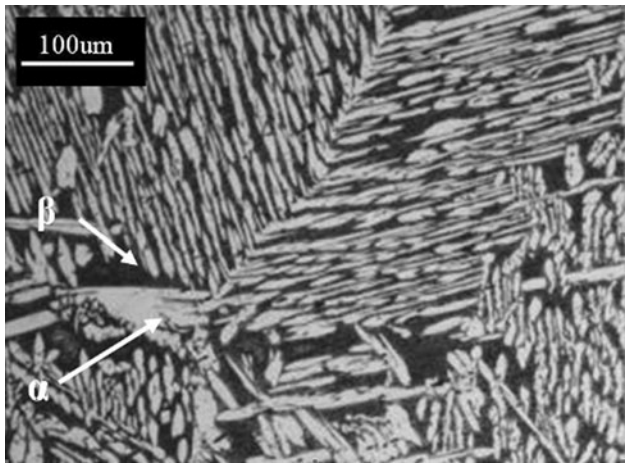

Fig. 5 As cast BM microstructure: optical image of etched specimen with EDS indication about phase detection)

temperature T_{L21} (Ref 16). In our case, the actual crystallographic structure of the β phase was not deeply investigated, because that goes beyond the scope of this work.

Furthermore, the investigations evidenced no phase differences between the bulk and the foamed samples, but a significant effect on grain size was observed. Grains were limited in their growth by the presence of the pores in the foamed materials, while they spread over several millimeters in the bulk specimens (Fig. 6, 7)

The image analysis method utilized for estimating the material porosity gave very reproducible results: average values are shown in Table 2. Measurements of the prismatic specimens confirmed these results. The porosity obtained with smaller space holders was found to be more regular and homogeneous over the whole foamed cylinder, compared to the case of foaming with bigger beads. The different foams showed an empty space proportion slightly higher than the reported 63-64%, which corresponds to random packing of shaken hard spheres of the same size. This result can be partially explained as a result of the non-complete wettability of silica-gel beads by molten brass that leaves part of the interstitial space unfilled, counterbalancing some piling faults (Ref 21).

Other reasons for this positive deviation of the theoretical space holder volume could be (Ref 22, 23) that: (a) the silica-gel beads are not perfectly spherical; (b) their size is not uniform; and (c) there is a localized contraction of the metal during the solidification.

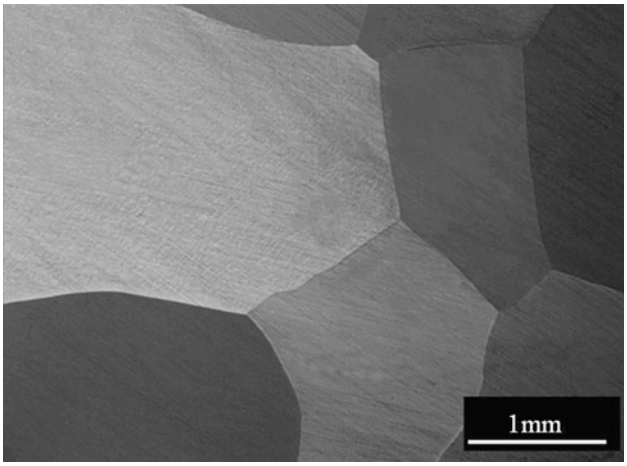

Fig. 6 Betatized bulk microstructure: austenitic phase (under polarized light)

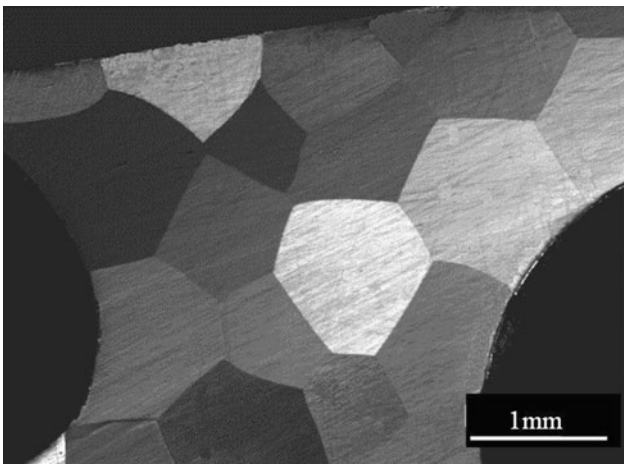

Fig. 7 Betatized foam microstructure: austenitic phase (under polarized light)

Table 2 Porosity and relative density of processed foams

	F3 (large pores)	F2 (medium pores)	F1 (small pores)
Average pore size, mm	4.5	3.4	2.5
Average porosity, %	68.7	64.7	65.9
Relative density	0.31	0.35	0.34

3.2 Calorimetric Measurement

Calorimetric analyses were conducted on samples of about 50 mg. The results show the M_s temperature, the transformation enthalpy (ΔH), and the thermal hysteresis of samples from the as-cast condition and after the betatization treatment. The values reported in Table 3 show transformation temperatures lower than room temperature, with comparable results in the different specimens. In the bulk (BM) betatized state, the investigated alloy has a sharp transformation peak, as depicted in Fig. 8. DSC scans of the F1 foam in as-cast condition and after betatization treatment are reported in Fig. 9. It is possible to observe that the betatization treatment improves the transformation behavior and shifts DSC peaks to higher temperatures, both in bulk and in foamed states. After the foaming process, broader transformation peaks are observed in the

Table 3 DSC results for a bulk specimen (betatized condition)

Specimen	A_s, °C	A_f, °C	$H_{heating}$, mJ/mg	M_s, °C	M_f, °C	$H_{cooling}$, mJ/mg
BM	−6.5	2.5	6.9	−9.5	−23	6.6
F1	−9	9.4	7.1	−7.6	−30.8	7.28
F2	−7.9	1.4	6.2	−9.2	−20	5.9
F3	−4.5	4.6	4.5	−1.5	−16.2	6.2

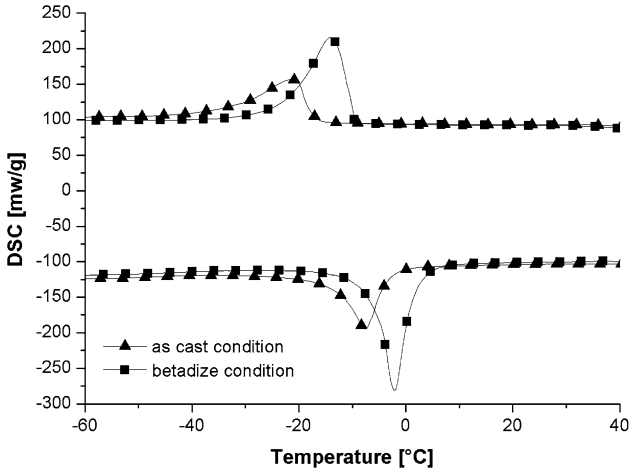

Fig. 8 DSC profiles of BM bulk specimens

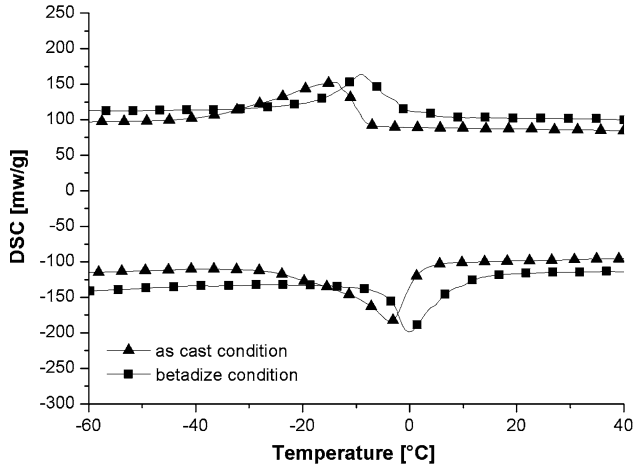

Fig. 9 DSC profiles of F1 foam specimens

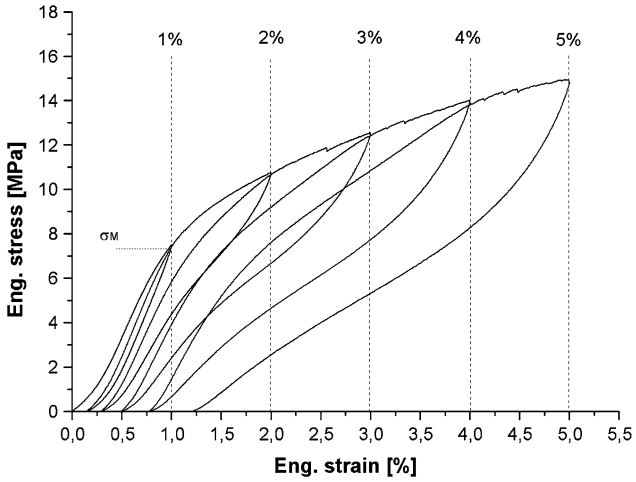

Fig. 10 PE compression test profiles; F1 foam specimen

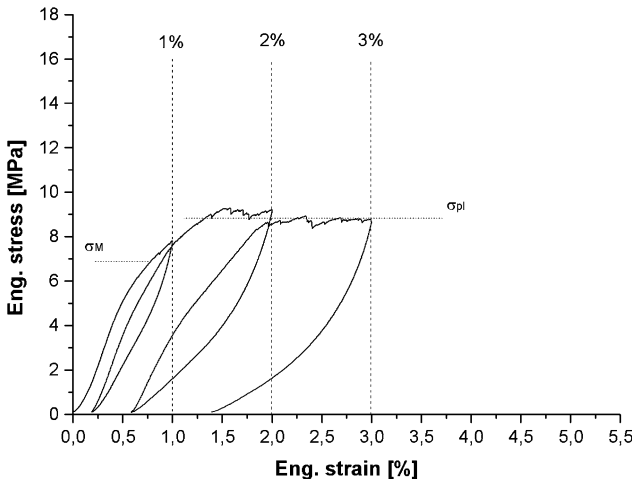

Fig. 11 PE compression test profiles; F3 foam specimens

temperature range reported in Table 3. All foam specimens (F1, F2, and F3) showed this same effect.

This phenomenon is likely connected with intrinsic in-homogeneities of the DSC specimens as those were taken from different locations in the SMA foam. In fact, possible discrepancies in the microstructure or morphology of the analyzed DSC samples may affect the intensity and shape of the peaks rather than the transformation onset and offset temperatures. Moreover, residual internal stresses, which could arise in the foamed SMA during water quenching and would change depending on space holders dimensions, may vary the peak intensities and, consequently, the transformation enthalpies. These results are confirmed by Ref 13.

All this suggests that using silica gel particles of different mean diameters to produce tailored morphologies in the synthesised specimens has no effects on the transformation behavior of the CuZnAl shape memory alloy.

3.3 Thermo-Mechanical Tests in Compression

PE and SME tests were carried out on samples of bulk metal and foams with different pore sizes on testing machine MTS RF/150.

PE tests were executed at the constant temperature of 30 °C, to maintain the material in the austenitic state, up to increasing levels of strain, at a deformation rate of 0.2 mm/min.

Bulk specimens, considered as the reference material, showed a complete recovery of strains up to 2%, but for increasing deformation levels, the residual strain became relevant; the critical stress for the induction of martensitic transformation is located around 150 MPa.

Foam specimens were not able to fully recover the applied strains even at low deformation levels, because of localized plasticity which can occur far below the overall compressive strength of the foam (Ref 5). Despite this fact, the ability to recover higher strains (over 4%) of foams with small pores (F1 foam) was better when compared to that of the bulk, probably because of irreversible sliding of grain surfaces occurring in the bulk samples (Fig. 10). Foams with large pores showed a low critical stress σ_{pl} (around 9 MPa), for collapsing of the pores: this is evident in the plateau-shaped stress-strain curves, which indicate irreversible deformation (Fig. 11).

Stress-induced martensite is formed above 7 MPa in foams with large pores, 9-10 MPa in foams with small pores; these results are well explained by a simple model scaling foams properties with porosity.

For a traditional foam (Ref 5):

$$\sigma_{pl} = \alpha_f \cdot \sigma_{y(bulk)} \cdot (1-p)^{3/2} \quad \text{(Eq 3)}$$

where σ_{pl} represents the critical densification stress in foamed state, $\sigma_{y(bulk)}$ is the yield stress of the bulk material and α_f is a constant equal to 0.3 ± 0.05. In a SMA metal foam, it is possible to assume:

$$\sigma_M = \alpha_f \cdot \sigma_{M(bulk)} \cdot (1-p)^{3/2} \quad \text{(Eq 4)}$$

where σ_M is the value of the stress necessary to induce martensite (SIM) in the foamed state, while $\sigma_{M(bulk)}$ is the SIM in the bulk.

The behavior of small-pores foam (F1) is in good accordance with the model (σ_{pl} = 13-14 MPa), while the critical stress is overestimated for foams with larger pores: this suggests that larger pores could prevent the achievement of a good pseudoelastic performance, because of premature collapsing of the structure. F2 foam shows intermediate features.

SME tests were carried out between 20 °C (T_0) and −30 °C (T_1). Cooling was obtained by injection of liquid nitrogen into

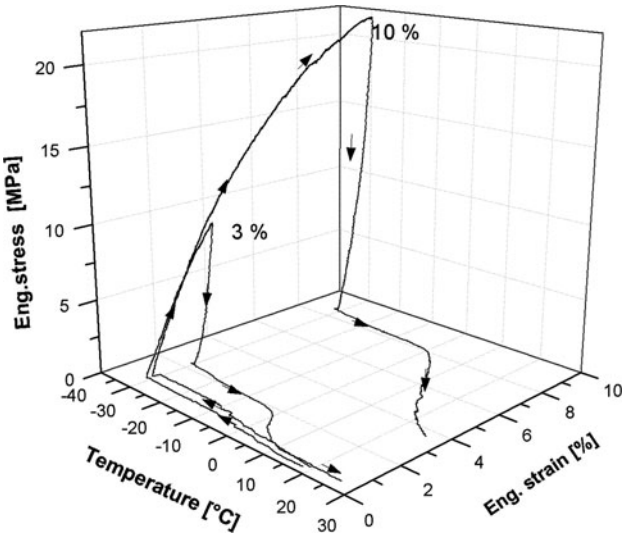

Fig. 12 SME compression test profiles; F1 foam specimen

the thermal chamber. The used preload was 50 N for foams and 100 N for bulk specimens, while deformation rate was 0.2 mm/min.

Bulk samples completely recovered applied strains of 3%, while after testing at 5%, a residual strain of 1% was detected. The F3 foam showed a not-neglectable 0.3% residual strain in the test at 3%, while after deformation at 5%, the total recovery was similar to that of the bulk. The F1 foam was tested with applied strains of 3 and 10% (Fig. 12): in the first case, deformation was recovered with quite small residual strain (0.17%); while in the second test, despite the high deformation level, more than 50% of the applied strain was recovered by shape-memory effect (nearly 70% if elastic recovery is considered). Again, the F2 foam showed intermediate features.

As observed in the PE tests, foamed samples showed worse performances at low strains (3%), but the foam with smallest pores gave very good results at higher strain levels; samples from foams with larger pores did not encounter, in the SME testing, the same severe premature collapse of the structure seen in the PE tests, probably because of a higher deformability of the martensitic phase at lower temperatures.

4. Conclusions

The results showed that metal foams of CuZnAl shape memory alloy can be reliably and advantageously produced with different pores size, using the proposed methodology (infiltration of molten metal among silica gel space-holders). The foaming process does not affect the microstructure of the alloy, but it has a refining effect on grain size; as observed in bulk samples, a betatization treatment (solubilization at 830 °C and water quenching) is needed to obtain a homogeneous microstructure. Porosity is found to be more homogeneous if smaller space-holders are used; measurements of this property by the image analysis method gave very reproducible results. Calorimetric analysis revealed no significant differences between bulk and foam samples; the main effects of the betatization treatment were found to be a shift in transformation temperatures to higher values and an increase in specific enthalpy. Mechanical behavior, as expected, is influenced by

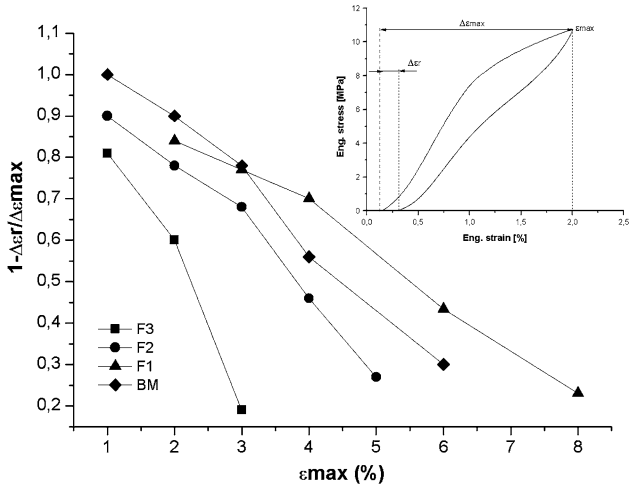

Fig. 13 PE compression tests summary results (*y*-axis represents an index of recovered strain)

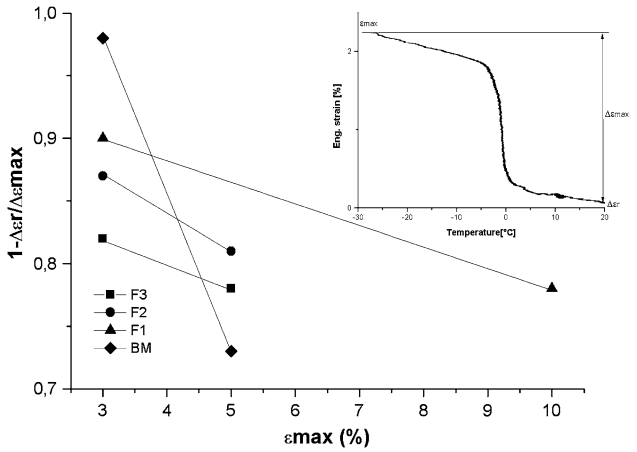

Fig. 14 SME compression tests summary results (*y*-axis represents an index of recovered strain)

the peculiar filled/void morphology of foams: pseudoelasticity and shape-memory effect were tested for both bulk and foam samples: a similar behavior is observed in both the cases, but stress levels are much different and scale with the relative density.

Collapsing of the foam structure occurs above a critical level σ_{pl}, which is found to be lower than expected (from scaling laws) for foams with larger pores; increase in pore size negatively affects the pseudoelastic behavior and gives rise to the observed plateau-shaped stress-strain curve in PE tests (irreversible deformation).

While at low strain levels (3%), pseudoelastic recovery of deformation is superior for bulk samples than for the foams, at higher strains the performance of small-pores foam is better, compared to the bulk.

Shape memory tests highlighted a similar trend: at low strains the bulk material offers better characteristics (3% strain is completely recovered), but at higher deformations it is outdone by the features of small-pores foams.

In summary, the functional properties of CZA foams with small pores seem to be better than those foams with larger pores (Fig. 13, 14), mainly because of the premature collapsing of the

pores occurring in the latter; a foaming process utilizing small space holders (around 2.5 mm) could enhance the thermomechanical behavior of a CZA shape memory alloy at high strain levels, thanks to a refining effect on the grain size, which prevents excessive sliding of grain boundaries.

Acknowledgments

The authors wish to thank Dr. Luca Signorelli (Politecnico of Milan) for his help in the mechanical characterization of the samples and Mr. Marco Pini (CNR IENI of Lecco) for foam specimen preparation.

References

1. A.G. Evans, J.W. Hutchinson, and M.F. Ashby, Multi Functionality of Cellular Metal Foams, *Prog. Mater. Sci.*, 1998, **43**(3), p 171–221
2. T.J. Lu, H.A. Stone, and M.F. Ashby, Heat Transfer in Open Cell Metal Foams, *Acta Mater.*, 1998, **46**(10), p 3619–3635
3. K.P. Dharmaseua and H.N.G. Wadley, Electrical Conductivity of Open-Cell Metal Foams, *J. Mater. Res.*, 2002, **17**(3), p 625–631
4. J. Banhart and J. Baumeister, Deformation Characteristic of Metal Foams, *J. Mater. Sci.*, 1999, **33**(6), p 1431–1440
5. M.F. Ashby, A. Evans, N.A. Fleck, L. Gibson, J.W. Hutchinson, and H. Wadley, *Metal Foams: A Design Guide*, Butterworth-Heinemann, Boston, 2000
6. J. Banhart, Manufacture, Characterization and Application of Cellular Metals and Metal Foams, *Prog. Mater. Sci.*, 2001, **46**, p 559–632
7. J. Banhart, Aluminium Foams for Lighter Vehicles, *Int. J. Vehic. Des.*, 2005, **37**(2–3), p 114–125
8. I. Duarte and J. Banhart, A Study of Aluminium Foam Formation—Kinetics and Microstructure, *Acta Mater.*, 2000, **48**(9), p 2349–2362
9. E. Andrews, W. Sander, and L.J. Gibson, Compressive and tensile behavior of aluminium foams, *Mater. Sci. Eng.*, 1999, **A270**, p 113–124
10. J. Banhart, Metallic Foams: Challenges and Opportunities, *Eurofoam2000*, P. Zitha, J. Banhart, and G. Verbist, Ed., MIT-Verlag, Bremen, 2000, p 13–20
11. H.N.G. Wadley, Cellular Metals Manufacturing, *Adv. Eng. Mater.*, 2002, **4**(10), p 726–733
12. E.M. Castrodeza and C. Mapelli, Processing of Brass Open-Cell Foam by Silica-Gel Beads Replication, *J. Mater. Process. Technol.*, 2009, **209**, p 4958–4962
13. E.M. Castrodeza, C. Mapelli, M. Vedani, S. Arnaboldi, P. Bassani, and A. Tuissi, Processing of Shape Memory CuZnAl Open-cell Foam by Molten Metal Infiltration, *J. Mater. Eng. Perform.*, 2009, **18**, p 484–489
14. M. Alhers, Martensite and Equilibrium Phase of the AlCuZn System for Compositions close to Brass Alloy, *Prog. Mater. Sci.*, 1986, **30**, p 135–186
15. J. Miettinen, Thermodynamic Description of the CuAlzn and CuSnZn Systems in the Copper Rich Corner, *Metall. Mater. Trans. A*, 2002, **26**(1), p 119–139
16. A. Planes, R. Romero, and M. Ahlers, The Martensitic Transition Temperature in Ternary CuZnAl Alloys. Influence of the L21 Structure, *Acta Metall. Mater.*, 1990, **38**(5), p 757–763
17. N. Kayaly, R. Zengin, and O. Adiguzel, Influence of Aging on Transformation Characteristic in Shape Memory CuZnAl Alloys, *Metall. Mater. Trans A*, 2000, **31A**, p 349–354
18. A. Cuniberti, R. Romero, and M. Stipcich, Stabilization Kinetics and Defects Retained by Quenching in 18R CuZnAl Martensite, *J. Alloy Compd.*, 2009, **472**, p 162–165
19. F.J. Gil, J.M. Guilemany, and J. Fernandez, Kinetic Grain Growth in Beta-Copper Shape Memory Alloys, *Mater. Sci. Eng. A*, 1998, **241**(1–2), p 114–121
20. E.E. Underwood, *Quantitative Stereology*, Addison Wesley Publishing Company, London, 1969
21. J.F. Despois, A. Marmottant, L. Salvo, and A. Mortensen, Spherical Pore Replicated Microcellular Aluminium: Processing and Influence on Properties, *Mater. Sci. Eng. A*, 2007, **462**(1-2), p 68–75
22. A.J. Matheson, Computation of a Random Packing of Hard Spheres, *J. Phys. C Solid State Phys.*, 1974, **7**(15), p 2569–2576
23. A. Donev, S. Torquato, F.H. Stillnger, and R. Cornelly, Jamming in Hard Sphere and Disk Packings, *J. Appl. Phys.*, 2004, **95**(3), p 989–999